Electronic structure of metallic ferromagnets above the Curie temperature

1985 J. Phys. F: Met. Phys. 15 1387

(http://iopscience.iop.org/0305-4608/15/6/019)

J. Phys. F: Met. Phys. **15** (1985) 1387–1404. Printed in Great Britain

Electronic structure of metallic ferromagnets above the Curie temperature

J Staunton†, B L Gyorffy‡, A J Pindor§, G M Stocks|| and H Winter¶

† Department of Physics, University of Warwick, Coventry CV4 7AL, UK
‡ H H Wills Physics Laboratory, University of Bristol, Bristol BS8 1TL, UK
§ Department of Physics, University of Toronto, Toronto, Canada
|| Metals and Ceramics Division, Oak Ridge National Laboratory, Oak Ridge, Tennessee 37831, USA
¶ Kernforschungszentrum Karlsruhe, Federal Republic of Germany

Received 20 June 1984

Abstract. We describe the electronic structure of Fe and Ni above their Curie temperatures in their disordered local moment (DLM) states as a function of wavevector $\boldsymbol{k}$ and energy ε. In particular, we calculate the Bloch spectral function, $\bar{A}(\boldsymbol{k}, \varepsilon)$, averaged over the orientational configurations of the local moments, at selected points in the Brillouin zone and determine the shape and smearing of the 'Fermi surface'. We find that BCC Fe, with a local moment of $1.9\,\mu_B$, can show an exchange splitting at some points whilst in other regions of the Brillouin zone no such splitting occurs. For comparison we also study FCC Fe, which also supports a substantial local moment. We find that it has similar features but the smearing of the 'bands' is more pronounced. On the other hand, the electronic structure of Ni is quite different, shows no such local exchange splitting, but is able to support a small local moment of $0.2\,\mu_B$. The resulting picture for the electronic structure of Ni is that of a paramagnetic smeared 'Stoner–Wohlfarth' model.

1. Introduction

In two previous papers (Pindor *et al* 1983, Gyorffy *et al* 1985, to be referred to as I and II respectively) we have developed a first-principles theory of ferromagnetic phase transitions in metals. In particular we have calculated the local moments supported by Cr, Fe, Co and Ni in the paramagnetic state as functions of temperature (I) and have studied the paramagnetic spin susceptibility of BCC Fe (II). In this paper we shall focus on features of the electronic structure which underlie their magnetic properties.

If the significance of these calculations is to be fully appreciated, it is important to place the subject of 'electronic structure above T_C' in the context of our current understanding of metallic magnetism. For a comprehensive review the reader is referred to the book edited by Moriya (1981). Here, we shall merely expand on the brief resumè given in II.

All modern theories are based upon a version of spin-polarised band theory and, then, attempt to include thermal fluctuations in the orientations of the local moments. Indeed, it is predominantly the entropy associated with these fluctuations which drives the transition to the paramagnetic state rather than that of the thermal excitation of electron–hole pairs as in the conventional Stoner–Wohlfarth theory. Whilst there is a general agreement on the broad outlines of this picture, there is controversy over the relative importance of the various thermally accessible, local moment configurations. On the one hand, proponents of

0305-4608/85/061387 + 18$02.25

the 'fluctuating local band' (FLB) picture (Korenman *et al* 1977, Prange and Korenman 1979, Capellmann 1974, 1979) would require large regions of near-aligned local moments even above T_C while, on the other hand, the disordered local moment (DLM) model (Hubbard 1979, 1981, Hasegawa 1979, Edwards 1982, Oguchi *et al* 1983, I, II) might have only a modest amount of short-range order (II) but more configurational entropy.

Clearly, in a satisfactory theory, the electronic and magnetic structure must determine each other self-consistently. Consequently, the assumption that the dominant magnetic fluctuations are different in the two approaches necessarily implies that the electronic structures are also different. Furthermore, modern experiments such as spin- and angle-resolved photoemission spectroscopy (SP-ARUPS) (Hopster *et al* 1983, Maetz *et al* 1982) and two-dimensional positron annihilation measurements (Berko 1979) are capable of determining the electronic structure directly, near T_C, in wavevector-dependent detail. Thus, such studies may contribute very usefully to our understanding of metallic magnetism at finite temperatures and may play an important role in resolving the conflicting views expressed by the FLB and DLM pictures. The present work was undertaken in order to encourage further experimental interest in this most promising field. Eventually, for a detailed comparison with such experiments, we hope that our results will provide input into calculations of photoemission spectra (Durham 1981) and momentum distribution functions (Gordon *et al* 1981, Szotek *et al* 1982), which have already been successful in interpreting experiments on disordered alloys but have not been studied in the present context.

The plan of the paper is as follows. Section 2 describes the conceptual framework within which 'band theory' at finite temperatures may be discussed; in § 3 there is a short summary of the relevant aspects of the theory in II and a brief description of the Bloch spectral function, $\bar{A}_B(\boldsymbol{k}, \varepsilon)$, is given. In § 4 we present and discuss the Bloch spectral functions at various points in $\boldsymbol{k}$ space for a range of energies for (*a*) BCC Fe, (*b*) FCC Fe and (*c*) FCC Ni in their DLM paramagnetic states and in § 5 the 'Fermi surfaces' are defined and described. Interpretation of the results in §§ 4 and 5 draws on concepts and insights gained from the study of the electronic structure of disordered alloys (Temmerman *et al* 1978, Gyorffy and Stocks 1979). Finally, in § 6 we comment on the implication of the overall picture which emerges from these calculations.

2. Electronic structure at finite temperatures

In this section we wish to clarify what we mean by the electronic structure at finite temperatures.

Single-particle properties of an interacting electron system at $T > 0$ are most efficiently described by the imaginary time, τ, Green function:

$$G(\boldsymbol{r}\tau, \boldsymbol{r}'0) = -\langle T(\psi(\boldsymbol{r}, \tau)\psi^{\dagger}(\boldsymbol{r}', 0))\rangle \tag{2.1}$$

where the operators $\psi^{\dagger}(\boldsymbol{r}', 0)$ and $\psi(\boldsymbol{r}, \tau)$ create and annihilate electrons at the space–imaginary-time points $(\boldsymbol{r}', 0)$ and $(\boldsymbol{r}, \tau)$ respectively and $\langle\ \rangle$ stands for an average over the usual Gibbsian ensemble (Fetter and Walecka 1971). Antiperiodicity of $G(\boldsymbol{r}\tau; \boldsymbol{r}', 0)$ with intervals 2β ensures that it may be written as a Fourier series

$$G(\boldsymbol{r}, \tau; \boldsymbol{r}'0) = \frac{1}{\beta}\sum_m G(\boldsymbol{r}, \boldsymbol{r}'; \mathrm{i}\varepsilon_m)\exp(-\mathrm{i}\varepsilon_m\tau) \tag{2.2}$$

over the Matsubara 'frequencies' $\varepsilon_m = (\pi/\beta)(2m+1)$ where $\beta^{-1} = k_B T$ and m is an integer. The quantity of interest here is the spectral function $\rho(\boldsymbol{r}, \boldsymbol{r}'; \varepsilon)$ defined by

$$G(\boldsymbol{r}, \boldsymbol{r}', \mathrm{i}\varepsilon_m) = \int_{-\infty}^{\infty} \frac{\mathrm{d}\varepsilon}{2\pi} \frac{\rho(\boldsymbol{r}, \boldsymbol{r}'; \varepsilon)}{\mathrm{i}\varepsilon_m - \varepsilon}. \tag{2.3}$$

It gives the most complete description of the one-particle spectra. While $G(\boldsymbol{r}, \boldsymbol{r}'; \mathrm{i}\varepsilon_m)$ is directly related to such equilibrium averages as the electron momentum distribution function

$$\begin{aligned} n(\boldsymbol{p}) &= \frac{1}{V} \beta^{-1} \sum_m \int^{\cdot} \mathrm{d}^3 r \int^{\cdot} \mathrm{d}^3 r' \exp[\mathrm{i}\boldsymbol{p} \cdot (\boldsymbol{r} - \boldsymbol{r}')] G(\boldsymbol{r}, \boldsymbol{r}'; \mathrm{i}\varepsilon_m) \exp(\mathrm{i}\varepsilon_m \eta) \\ &= \beta^{-1} \sum_m G(\boldsymbol{p}, \boldsymbol{p}; \mathrm{i}\varepsilon_m) \exp(\mathrm{i}\varepsilon_m \eta) \end{aligned} \tag{2.4}$$

where V is the total volume of the sample and η is an infinitesimal quantity to be set equal to zero after the sum over m has been performed, the spectral function $\rho(\boldsymbol{r}, \boldsymbol{r}'; \varepsilon)$ also determines the various real-time Green functions (Fetter and Walecka 1971). These latter are probed by angle-resolved photoemission spectroscopy in wavevector-dependent detail and $n(\boldsymbol{p})$ can be studied in positron annihilation experiments. Indeed, these two are the experiments to which this investigation is most relevant.

The invariance of the equilibrium ensemble under the translation group of the Bravais lattice implies that

$$G(\boldsymbol{r} + \boldsymbol{R}, \boldsymbol{r}' + \boldsymbol{R}; z) = G(\boldsymbol{r}, \boldsymbol{r}'; z) \tag{2.5}$$

where $\boldsymbol{R}$ is an arbitrary lattice vector. Hence it is convenient to work in reciprocal space.

While useful, the real momentum spectral function

$$\rho(\boldsymbol{p}, \varepsilon) = -(1/\pi) \operatorname{Im} G(\boldsymbol{p}, \boldsymbol{p}; z = \varepsilon + \mathrm{i}\eta) \tag{2.6}$$

carries too much wavefunction-dependent information for our purpose. This is clear from the fact that $\rho(\boldsymbol{p}, \varepsilon)$ is not periodic in reciprocal space as the spectrum should be. The quantity nearest to providing a 'band structure' type description is the Bloch spectral function defined by

$$\bar{A}_B(\boldsymbol{k}, \varepsilon) = \sum_k \rho(\boldsymbol{k} + \boldsymbol{K}; \varepsilon). \tag{2.7}$$

At $T = 0$ in a one-electron approximation $\bar{A}_B(\boldsymbol{k}, \varepsilon)$ consists of a set of δ-function peaks:

$$\bar{A}_B(\boldsymbol{k}, \varepsilon) = \sum_\nu \delta(\varepsilon - \varepsilon_{\boldsymbol{k}, \nu})$$

at the Bloch energy eigenvalues $\varepsilon_{\boldsymbol{k}, \nu}$ where ν is the band index. In a fully interacting theory they broaden into quasiparticle peaks except on the Fermi surface at $T = 0$ where the quasiparticle lifetime is infinite. Although the one-electron excitations are not exact eigenstates of the many-body system the peaks of $\bar{A}_B(\boldsymbol{k}, \varepsilon)$ may be expected to be well defined on the scale of their separation in energy. Under these circumstances it is useful to think of them as defining Bloch states (Dyson orbitals) with finite lifetimes. Thus we shall take $\bar{A}_B(\boldsymbol{k}, \varepsilon)$ as a description of the finite-temperature band structure and study it near the Curie point ($T_C \sim 10^3$ K). The approximation we shall use arises from the DLM picture developed in I and II and will be described in the next two sections.

It identifies the scattering of electrons from the thermal fluctuations of the local polarisation as the dominant mechanism of broadening near T_C. Loosely speaking, the picture is that of quasiparticles dressed by the combined influence of Stoner electron–hole excitations together with the collective spin fluctuation effects given by this local moment picture.

3. The disordered local moment approximation

Of course, present-day 'band theory means' do not provide a prescription for the Bloch spectral function $\bar{A}_B(\boldsymbol{k}, \varepsilon)$ defined above. Whilst many-body diagram summation techniques do give us a recipe for calculating $\bar{A}_B(\boldsymbol{k}, \varepsilon)$ these have proved tractable only for grossly simplified model interactions. Thus up till now little has been known about $\bar{A}_B(\boldsymbol{k}, \varepsilon)$ at finite temperatures quantitatively. In what follows we shall present an approximation scheme for evaluating $\bar{A}_B(\boldsymbol{k}, \varepsilon)$ from first principles in quantitative detail. In short our approach is that of I and II where, implicitly, we had all the information to study $\bar{A}_B(\boldsymbol{k}, \varepsilon)$.

The argument is most succinct if we rewrite $\bar{A}_B(\boldsymbol{k}, \varepsilon)$ as

$$\bar{A}_B(\boldsymbol{k}, \varepsilon) = -\frac{1}{\pi} \operatorname{Im} \frac{1}{V} \sum_{\boldsymbol{K}} \int d^3 r \int d^3 r' \exp[-i(\boldsymbol{k}+\boldsymbol{K}) \cdot (\boldsymbol{r}-\boldsymbol{r}')] G(\boldsymbol{r}, \boldsymbol{r}'; \varepsilon + i\eta)$$

$$= -\frac{1}{\pi} \operatorname{Im} \frac{1}{V} \sum_{i,j} \int_{V_i} d^3 \boldsymbol{r}_i \int_{V_i} d\boldsymbol{r}_j' \exp[-i(\boldsymbol{k}+\boldsymbol{K}) \cdot (\boldsymbol{r}_i - \boldsymbol{r}_j' + \boldsymbol{R}_i - \boldsymbol{R}_j)] \tag{3.1}$$

$$\times G(\boldsymbol{r}_i + \boldsymbol{R}_i, \boldsymbol{r}_j' + \boldsymbol{R}_j; \varepsilon + i\eta)$$

$$= -\frac{1}{\pi} \operatorname{Im} \sum_j \exp[i(\boldsymbol{k}+\boldsymbol{K}) \cdot (\boldsymbol{R}_j - \boldsymbol{R}_i)] \frac{1}{V_i} \int d^3 r_i G(\boldsymbol{r}_i, \boldsymbol{r}_i + \boldsymbol{R}_j - \boldsymbol{R}_i; \varepsilon + i\eta) \tag{3.2}$$

where we have used equation (2.5) and the identity $\Sigma_{\boldsymbol{K}} \exp[i\boldsymbol{K} \cdot (\boldsymbol{r}_i - \boldsymbol{r}_j')] = \delta(\boldsymbol{r}_i - \boldsymbol{r}_j')$. The volume of the ith unit cell is denoted by V_i to emphasise the absolute location of the region of spatial integration and is taken to be the same, V_0, all through the sample. It is for $G(\boldsymbol{r}, \boldsymbol{r}+\boldsymbol{R}; \varepsilon^+)$ that we shall develop our theory.

The argument in II was based on the supposition that it is useful to distinguish between the fast time scale of electrons hopping from site to site and the slower time scale on which the local spin polarisation, the local moment, changes its direction. Accordingly, a unit vector $\hat{\boldsymbol{e}}_i$ was assigned to each site i to represent the direction of spin polarisation averaged over a time τ long compared with the hopping time $\hbar/W$, where W is an effective band width, but short compared with an inverse spin-wave frequency $1/\omega_s$. For times less than τ the system was described by a finite-temperature density functional theory (Rajagopal 1980) in the local density approximation for a fixed orientational configuration $\{\hat{\boldsymbol{e}}_i\}$. Then it was imagined that the subsequent slow time evolution of the configuration $\{\hat{\boldsymbol{e}}_i\}$ is ergodic and therefore may be replaced by an average over all configurations with an appropriate statistical weight.

In short, the method is to break up the process of averaging an operator $\hat{o}$ with respect to the full equilibrium density matrix of the electron system ρ into two parts:

$$\langle \hat{o} \rangle = \operatorname{Tr}(\rho \hat{o}) = \frac{1}{Z} \sum_{\{\hat{\boldsymbol{e}}_i\}} \exp[-\beta \Omega(\{\hat{\boldsymbol{e}}_i\})] \operatorname{Tr}(\rho(\{\hat{\boldsymbol{e}}_i\}) \hat{o}) \tag{3.3}$$

in which the first part is an average with respect to the density matrix $\rho(\{\hat{e}_i\})$ such that the corresponding average magnetisation $\boldsymbol{m}(\boldsymbol{r}, \{\hat{e}_i\})$ satisfies the constraint

$$\int_{\Omega_i} \mathrm{d}^3 r\, \boldsymbol{m}(\boldsymbol{r}; \{\hat{e}_i\}) \times \hat{e}_i = 0 \tag{3.4}$$

(i.e. its spatial average over the ith unit cell is along $\hat{e}_i$), and the second part is a statistical sum with respect to the collective variables $\{\hat{e}_i\}$ and the measure determined by the grand potential $\Omega(\{\hat{e}_i\})$ corresponding to $\rho(\{\hat{e}_i\})$.

The non-equilibrium density matrix $\rho(\{\hat{e}_i\})$ is determined by the condition that it minimises

$$\Omega[\rho] = \mathrm{Tr}\,(\rho[\hat{H} - \nu\hat{N} + (1/\beta)\ln\rho]) \tag{3.5}$$

where $\hat{H}$ and $\hat{N}$ are the Hamiltonian and number operators respectively and ν is the chemical potential, and simultaneously satisfies the constraint given in equation (3.4). The grand potential for a given orientational configuration, $\Omega(\{\hat{e}_i\})$, is obtained by evaluating $\Omega[\rho]$ for $\rho(\{\hat{e}_i\})$ and

$$Z = \sum_{\{\hat{e}_i\}} \exp[-\beta\Omega(\{\hat{e}_i\})]. \tag{3.6}$$

As the next step in the scheme, a density functional theory is developed for $\Omega(\{\hat{e}_i\})$ and any average of the form $\langle\hat{o}\rangle_{\{\hat{e}_i\}} \equiv \mathrm{Tr}(\rho(\{\hat{e}_i\})\hat{o})$. In particular $G(\boldsymbol{r}, \boldsymbol{r}'; \varepsilon; \{\hat{e}_i\})$ is approximated by the Green function of the finite-temperature version of the Kohn–Sham equations with the exchange–correlation potential at each site, $\mathbf{v}_i^{\mathrm{xc}}(\boldsymbol{r} - \boldsymbol{R}_i)$, constrained to be of the form

$$\mathbf{v}_i^{\mathrm{xc}}(\boldsymbol{r} - \boldsymbol{R}_i) = v_i^{\mathrm{xc}}(\boldsymbol{r} - \boldsymbol{R}_i)\mathbf{1} + w^{\mathrm{xc}}(\boldsymbol{r} - \boldsymbol{R}_i)\hat{e}_i \cdot \boldsymbol{\sigma} \tag{3.7}$$

where v^{xc} and w^{xc} are the usual von Barth and Hedin (1972) local spin-density approximate functionals of the charge density and magnetisation.

Thus, the Green function to be used in equation (3.2) is given by

$$\begin{aligned} G(\boldsymbol{r}, \boldsymbol{r}'; \mathrm{i}\varepsilon_m) &= \langle G(\boldsymbol{r}, \boldsymbol{r}'; \mathrm{i}\varepsilon_m; \{\hat{e}_i\})\rangle \\ &= \frac{1}{Z}\prod_i \int_{\Omega_i} \mathrm{d}\hat{e}_i \exp(-\beta\Omega(\{\hat{e}_i\}))G(\boldsymbol{r}, \boldsymbol{r}'; \mathrm{i}\varepsilon_m; \{\hat{e}_i\}) \end{aligned} \tag{3.8}$$

where the partition function Z is that given in equation (3.6).

Finally, the statistical sum in equation (3.8) is carried out in the mean-field approximation using the self-consistent Korringa–Kohn–Rostoker coherent-potential-approximation (KKR CPA) scheme (Winter and Stocks 1983). The details of this last step will be elaborated in the next section.

From the point of view of the present paper the above procedure implies an extra approximation in addition to those in I and II. There $G(\boldsymbol{r}, \boldsymbol{r}'; \mathrm{i}\varepsilon_m)$ was only used for calculating the charge density, the magnetisation density and the grand potential. The legitimacy of these applications is guaranteed by the fundamental tenets of the density functional theory. Here, on the other hand, we wish to use the spectral function $\rho(\boldsymbol{r}, \boldsymbol{r}'; \varepsilon)$ to discuss the whole spectrum. Namely, we interpret $\bar{A}_B(\boldsymbol{k}, \varepsilon)$ as a description of the excited states as well as the basis for calculating equilibrium properties. In principle, there are no grounds for such an interpretation. Nevertheless, we recall that the eigenvalues and eigenfunctions of the Kohn–Sham equations at $T = 0$ have given a useful guide to the excitation spectrum at low temperatures even in the case of the photoemission process

which involves highly excited states. Thus we proceed to investigate the consequences of disregarding the injunctions of the density functional theorem against the use of its Euler–Lagrange equation as a Dyson equation in the new regime of high temperatures with the hope that it might again lead to more insight than confusion.

4. The mean-field theory of the DLM state

In II we have shown that the mean-field approximation for the statistical sum in equation (3.6) is

$$Z=\prod_i Z_i=\prod_i \int_{\hat{e}_i} \mathrm{d}\hat{e}_i \exp(-\beta\omega_i(\hat{e}_i)) \tag{4.1}$$

where $\omega_i(\hat{e}_i)$ is the partial average of the grand potential $\Omega(\{\hat{e}_i\})$,

$$\omega_i(\hat{e}_i)=\langle\Omega(\{\hat{e}_i\})\rangle_{\hat{e}_i}, \tag{4.2}$$

with respect to the inhomogeneous product distribution function

$$P(\{\hat{e}_i\})=\prod_i \frac{1}{Z_i}\exp(-\beta\omega_i(\hat{e}_i)). \tag{4.3}$$

These three equations are a set of self-consistency requirements on the local orientation distribution function:

$$P_i(\hat{e}_i)=\frac{1}{Z_i}\exp(-\beta\omega_i(\hat{e}_i)) \tag{4.4}$$

which determine $\omega_i(\hat{e}_i)$ and hence $P_i(\hat{e}_i)$ uniquely. To solve them for $\omega_i(\hat{e}_i)$ we must know the partial average

$$\langle\Omega(\{\hat{e}_i\})\rangle_{\hat{e}_i}=\prod_{j\neq i}\int_{\hat{e}_j} \mathrm{d}\hat{e}_j\, P_j(\hat{e}_j)\Omega(\{\hat{e}_i\}) \tag{4.5}$$

as a function of the set $\{\omega_i\langle\hat{e}_i\rangle\}$. In II we have argued that the spirit of the mean-field theory requires that the averaging involved in the calculation of $\langle\Omega\rangle_{\hat{e}_i}$ is to be carried out in the CPA. By inverting the order of averaging and the achievement of the charge and magnetisation density self-consistency required by the spin-density functional theory for the states with the prescribed orientation $\{\hat{e}_i\}$, we have arrived at the following self-consistent field (SCF) inhomogeneous KKR CPA scheme.

(*a*) We begin with a density matrix which depends only on the local orientation $\hat{e}_i$ assigned to each site. It is taken to be of the form

$$\bar{\mathbf{n}}_i(\boldsymbol{r};\hat{e}_i)=\bar{n}_i(\boldsymbol{r};\hat{e}_i)+\bar{\mu}_i(\boldsymbol{r};\hat{e}_i)\boldsymbol{\sigma}\cdot\hat{e}_i \tag{4.6}$$

where $\bar{n}_i(\boldsymbol{r};\hat{e}_i)$ is the local charge density, $\bar{\mu}(\boldsymbol{r};\hat{e}_i)\hat{e}_i$ is the local magnetisation density, constrained to be parallel to $\hat{e}_i$ and $\boldsymbol{\sigma}^x$, $\boldsymbol{\sigma}^y$ and $\boldsymbol{\sigma}^z$ are the usual Pauli spin matrices.

(*b*) From $\bar{\mathbf{n}}_i(\boldsymbol{r};\hat{e}_i)$ we calculate a set of potential functions $\bar{\mathbf{v}}_i(\boldsymbol{r}-\boldsymbol{R}_i)$ following the prescription of the local spin density (LSD) approximation (von Barth and Hedin 1972).

(*c*) Then we solve for the partially averaged Green function $\langle\mathbf{G}(\boldsymbol{r},\boldsymbol{r}';\varepsilon;\{\hat{e}_i\})\rangle_{\hat{e}_i}$ where $\mathbf{G}(\boldsymbol{r},\boldsymbol{r}';\varepsilon;\{\hat{e}_i\})$ satisfies the Kohn–Sham–Mermin Pauli equation

$$\left[\left(\varepsilon+\frac{\hbar}{2m}\nabla^2\right)\mathbf{1}+\sum_i \bar{\mathbf{v}}_i(\boldsymbol{r}-\boldsymbol{R}_i;\hat{e}_i)\right]\mathbf{G}(\boldsymbol{r},\boldsymbol{r}';\varepsilon;\{\hat{e}_i\})=\mathbf{1}\delta(\boldsymbol{r}-\boldsymbol{r}') \tag{4.7}$$

using an inhomogeneous KKR CPA ansatz corresponding to the distribution function in equation (4.3). This gives us the partially averaged local density matrix

$$\langle \bar{\mathbf{n}}_i(\boldsymbol{r}; \{\hat{e}_i\})\rangle_{\hat{e}_i} = -\frac{1}{\pi}\int \mathrm{d}\varepsilon\, f(\varepsilon)\, \mathrm{Im}\langle \mathbf{G}(\boldsymbol{r}, \boldsymbol{r}; \varepsilon; \{\hat{e}_i\})\rangle_{\hat{e}_i}. \tag{4.8}$$

(*d*) The final step, which makes the calculation self-consistent on the average, is to identify the starting density matrix $\bar{\mathbf{n}}_i(\boldsymbol{r}; \hat{e}_i)$ with the partially averaged density matrix $\langle \bar{\mathbf{n}}_i(\boldsymbol{r}; \{\hat{e}_i\})\rangle_{\hat{e}_i}$ and iterate to self-consistency. Note that at the end of such a calculation we have a set of local moments

$$\bar{\mu}_i(\hat{e}_i) = \int_{V_i} \mathrm{d}^3 r_i\, \bar{\mu}_i(\boldsymbol{r}_i; \hat{e}_i) \tag{4.9}$$

which, in principle, can vary from site to site and be a function of the local orientation $\hat{e}_i$.

(*e*) The partially averaged grand potential $\langle \Omega(\{\hat{e}_i\})\rangle_{\hat{e}_i}$ is calculated by integrating with respect to the chemical potential the partially averaged integral of the particle density

$$\langle \bar{N}(\{\hat{e}_i\})\rangle_{\hat{e}_i} = \int_{V_i} \mathrm{d}^3\, r(\bar{n}_i(\boldsymbol{r}; \hat{e}_i) - \langle \bar{n}_i(\boldsymbol{r}; \hat{e}_i)\rangle) + \sum_{j\neq i}\int_{V_j} \mathrm{d}^3 r \langle \bar{n}_j(\boldsymbol{r}; \hat{e}_j)\rangle \tag{4.10}$$

where

$$\langle \bar{n}_j(\boldsymbol{r}; \hat{e}_j)\rangle = \int \mathrm{d}^2\hat{e}_j\, P_j(\hat{e}_j)\bar{n}(\boldsymbol{r}; \hat{e}_j). \tag{4.11}$$

Namely,

$$\langle \Omega(\{\hat{e}_i\})\rangle_{\hat{e}_i} \equiv \omega_i^{(1)}(\hat{e}_i) = -\int_{-\infty}^{\nu} \mathrm{d}\nu'\, \langle \bar{N}(\{\hat{e}_i\}, \nu')\rangle_{\hat{e}_i}. \tag{4.12}$$

To be fully explicit we now describe briefly the KKR CPA procedure which takes one from equation (4.7) to equation (4.8).

The potential well described by $\bar{\mathbf{v}}_i(\boldsymbol{r}; \hat{e}_i)$ is assumed to be of the usual muffin-tin form and diagonal in spin space if the axis of quantisation is taken along $\hat{e}_i$. Thus it is of the form

$$\bar{\mathbf{v}}_i(\boldsymbol{r}, \hat{e}_i) = \tfrac{1}{2}(\bar{v}_+(\boldsymbol{r}, \hat{e}_i) + \bar{v}_-(\boldsymbol{r}; \hat{e}_i))\mathbf{1} + \tfrac{1}{2}(\bar{v}_+(\boldsymbol{r}; \hat{e}_i) - \bar{v}_-(\boldsymbol{r}, \hat{e}_i))\boldsymbol{\sigma}\cdot\hat{e}_i \tag{4.13}$$

where $\bar{v}_+$ is the potential 'seen' by an electron with spin parallel to $\hat{e}_i$ and $\bar{v}_-$ is that for an electron whose spin is antiparallel to $\hat{e}_i$. From $\bar{\mathbf{v}}_i(\boldsymbol{r}; \hat{e}_i)$ we calculate the 'on the energy shell' partial-wave t matrix:

$$\mathbf{t}_{i,L}(\varepsilon; \hat{e}_i) = \tfrac{1}{2}(t_{L,+}(\varepsilon; \hat{e}_i) + t_{L,-}(\varepsilon; \hat{e}_i))\mathbf{1} + \tfrac{1}{2}(t_{L,+}(\varepsilon; \hat{e}_i) - t_{L,-}(\varepsilon; \hat{e}_i))\boldsymbol{\sigma}\cdot\hat{e}_i \tag{4.14}$$

where L stands for both the polar, l, and azimuthal, m, quantum numbers.

The CPA medium is defined as a lattice of effective scatterers described by the effective t matrix $\mathbf{t}_{c,i,L}(\varepsilon)$. The scattering of an electron at an impurity, corresponding to $\mathbf{t}_{i,L}(\varepsilon, \hat{e}_i)$ in this medium, is completely determined by the scattering matrix:

$$\boldsymbol{\tau}^{\hat{e}_i; ii} = [\mathbf{1} - (\mathbf{t}_{c,i}^{-1} - \mathbf{t}_i^{-1})\boldsymbol{\tau}^{c,ii}]^{-1}\boldsymbol{\tau}^{c,ii} \tag{4.15}$$

where all the symbols are matrices with labels L and L' as well as spin-space matrices and the usual rules of matrix multiplication are implied. The single-site t matrix of the medium $\boldsymbol{\tau}^{c,ij}$ is the solution of the multiple scattering equation

$$\sum_l (\mathbf{t}_{c,i}^{-1}\delta_{i,l} - \mathbf{G}(\boldsymbol{R}_i - \boldsymbol{R}_j; \varepsilon))\boldsymbol{\tau}^{c,lj} = \mathbf{1}\delta_{ij}. \tag{4.16}$$

Thus, the CPA condition, which determines $\mathbf{t}_{c,i,L}$ is given by

$$\int d^2\hat{e}_i \, P_i(\hat{e}_i) \, \boldsymbol{\tau}^{\hat{e}_i;ii}(\varepsilon) = \mathbf{1}. \tag{4.17}$$

When looking for a ferromagnetic state all the sites are taken to be equivalent. Namely $\omega_i(\hat{e}_i) = \omega(\hat{e}_i)$, $P_i(\hat{e}_i) = P_0(\hat{e}_i)$, $\mathbf{t}_{c,i,L} = \mathbf{t}_{c,L}$ for all i and

$$\boldsymbol{m}_i = \boldsymbol{m} = \langle \hat{e}_i \rangle = \int d\hat{e}_i \, P_0(\hat{e}_i)\hat{e}_i. \tag{4.18}$$

Under these circumstances the above scheme can be readily implemented. In II we have shown how the temperature T_C at which the $\boldsymbol{m}=0$ state becomes unstable can be found and how the static susceptibility $\chi(\boldsymbol{q})$ is determined.

In the present paper we focus on the electronic structure in the paramagnetic state, $\boldsymbol{m}=0$. As we have shown in I and II, in that case $P_0(\hat{e}) = 1/4\pi$ as might have been expected on the grounds of symmetry. Then it is sufficient to take $\hat{e}_i$ to be an Ising-like variable: $\hat{e}_i^x = \hat{e}_i^y = 0$ and $\hat{e}_i^z = \pm 1$. Consequently, equation (4.17) takes the form

$$\tfrac{1}{2}[\mathbf{1} + (\mathbf{t}^{-1}(\uparrow) - \mathbf{t}_c^{-1})\boldsymbol{\tau}^{c,ii}]^{-1} + \tfrac{1}{2}[\mathbf{1} + (\mathbf{t}^{-1}(\downarrow) - \mathbf{t}_c^{-1})\boldsymbol{\tau}^{c,ii}]^{-1} = \mathbf{1} \tag{4.19}$$

where again we have suppressed the angular momentum labels. In fact, because we work with $l_{max} \leqslant 2$ and the lattice is cubic $\mathbf{t}(\uparrow)$, $\mathbf{t}(\downarrow)$, $\mathbf{t}_c$ and $\boldsymbol{\tau}^{c,ii}$ are all diagonal in L. Moreover, they are diagonal in spin space. Nevertheless, if there is local exchange splitting, for example a local moment, $t_{c,+,+} \neq t_{c,-,-}$ and $\boldsymbol{\tau}^{c,ii}_{+,+} \neq \boldsymbol{\tau}^{c,ii}_{-,-}$.

In I we have solved (4.19) numerically and iterated the full calculation to self-consistency in the sense of (*a*), (*b*), (*c*) and (*d*) for Cr, Fe, Co and Ni using their experimentally observed crystal structure. Here we shall report our calculations for FCC Fe as well.

Finally, we return to our main concern—the Bloch spectral function $\bar{A}_B(\boldsymbol{k};\varepsilon)$ defined in § 2. Evidently, the approximation to $G(\boldsymbol{r},\boldsymbol{r}';i\varepsilon_m)$ given in equation (3.8) is to be our starting point. In the mean-field approximation of § 4 $\langle G(\boldsymbol{r},\boldsymbol{r}';i\varepsilon_m;\{\hat{e}_i\})\rangle$ is given by the CPA solution of equation (4.8). Thus we need to work out $\bar{A}_B(\boldsymbol{k},\varepsilon)$ defined in equation (3.2), the CPA-averaged Green function. The derivation of a CPA formula for $\bar{A}_B(\boldsymbol{k},\varepsilon)$ follows closely the argument of Faulkner and Stocks (1980) and is given in the appendix. All our calculations were performed by evaluating the expression for $\bar{A}_B(\boldsymbol{k},\varepsilon)$ in the appendix using our solution of equation (4.19) and the radial solutions of the Schrödinger equation corresponding to our self-consistently determined potential functions $\bar{\mathbf{v}}(\boldsymbol{r};\uparrow)$ and $\bar{\mathbf{v}}(\boldsymbol{r},\downarrow)$.

It is fruitful to note, at this stage, that the above calculations are entirely analogous to those for random binary alloys with v_A and v_B, playing the role of $\mathbf{v}(\uparrow)$ and $\mathbf{v}(\downarrow)$, describing the crystal potential of an alloy with species named A and B respectively. Thus, our efforts to include non-local spin correlations into the LSD approximation lead to the same kind of alloy analogy as was exploited by Hubbard (1963) in connection with his simplified many-body Hamiltonian. Nevertheless it should be stressed that while the alloy analogy in the context of the Hubbard model approximates correlation fluctuations about the Hartree–Fock solution, in the present theory it describes fluctuations about the LSD approximation to the equilibrium state. Since this latter is more securely founded, both in principle and in terms of practical calculations, than the Hartree–Fock solution to the Hubbard Hamiltonian our scheme should be more reliable.

There is another reason for noting this analogy between fluctuating Ising-like moments and compositional fluctuations in a random binary alloy. This is to do with the fact that

this latter theory is quite well developed and much useful insight into the working of the CPA is available.

It is thus convenient to introduce some concepts from alloy theory which will prove useful in interpreting the plots of $\bar{A}_B(\boldsymbol{k}, \varepsilon)$ (shown in the following sections). In various regions of $\boldsymbol{k}$ and energy space, the behaviour of $\bar{A}_B(\boldsymbol{k}, \varepsilon)$ can be classified into two broad categories: (i) when two broadened peaks occur, one peak loosely associated with an 'up' site state and the other with the corresponding 'down' site state—this is termed 'split band' behaviour; and (ii) when a single smeared peak appears between these two states—this is 'virtual crystal' behaviour. We will elaborate on these phrases: with the simplest tight-binding models, the CPA will produce the latter 'virtual crystal' type features if the centres of mass of the densities of states from ordered lattices of all 'up' potentials and all 'down' potentials are close in energy compared with their band widths, and 'split band' if not. At a given $\boldsymbol{k}$ point, however, it is difficult to express similar ideas about the KKR CPA Bloch spectral function $\bar{A}_B(\boldsymbol{k}, \varepsilon)$. Experience with alloys has shown that a useful interpretative gauge to construct can be derived from the fictitious band structures calculated by placing an 'up' potential and then a 'down' Fe potential on every lattice site. Frequently then, given the separation of two corresponding states from these ordered systems, the 'up' and 'down' pure band structures will naturally suggest an appropriate energy scale or local width on which to assess this difference. Such a local scale is $\hbar|\nabla\varepsilon_{\boldsymbol{k}}|$ and from this one can fairly reliably predict the qualitative features of $\bar{A}_B(\boldsymbol{k}, \varepsilon)$ for the disordered systems. It is for these reasons that we show the interpretative gauges of figures 1, 2 and 3. Figure 1 shows the fictitious bands in the Γ–H direction that an electron with spin $+\frac{1}{2}$ 'sees' in a lattice of (*a*) 'up' and (*b*) 'down' Fe potentials. Figure 2 shows similar bands for FCC Fe in the Γ–X direction and figure 3 shows those for FCC Ni. An electron with spin $-\frac{1}{2}$ will 'see' the same bands with the labels 'up' and 'down' interchanged.

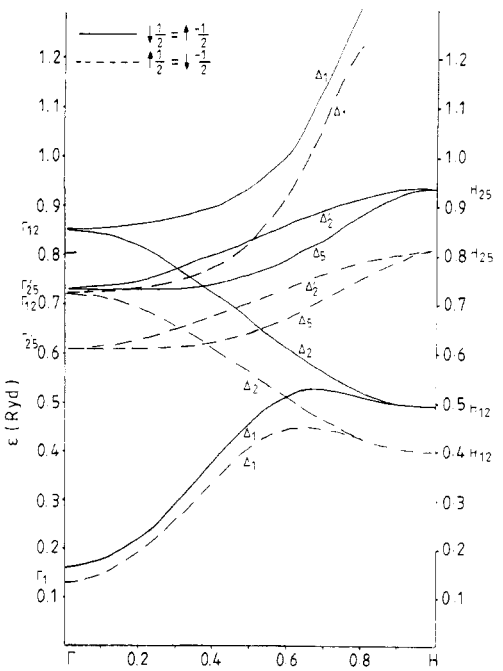

Figure 1. Band structures of fictitious systems with SCF KKR CPA 'up' (broken curves) and 'down' (full curves) potentials placed on every lattice site ($a_0 = 5.27$ au) from a calculation for BCC Fe ($T = 1200$ K) for the Δ direction.

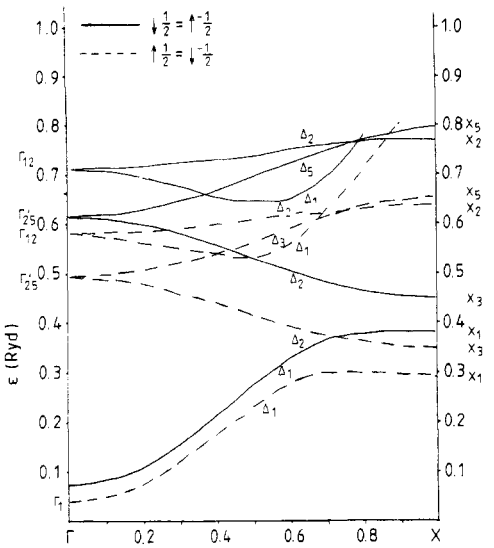

Figure 2. As figure 1 but for FCC Fe ($a_0 = 6.88$ au, $T = 1200$ K) for the Δ direction.

The following two sections give a description and interpretation using the above guidelines for the Bloch spectral functions of Fe and Ni.

5. Constant-k Bloch spectral functions for Fe and Ni

In I SCF KKR CPA calculations for Fe, Ni, Co and Cr were described for a range of temperatures and, in the case of Fe and Ni, with different lattice spacings. The local moment established in Ni was found to be very sensitive to both temperature and lattice

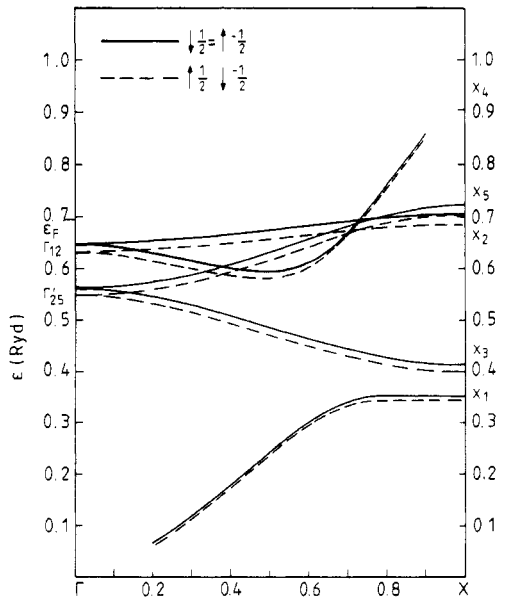

Figure 3. As figure 1 but for FCC Ni ($a_0 = 6.55$ au, $T = 10$ K).

dimensions. In this section we describe details of the electronic structure resulting from some of that work. We look at BCC Fe on a lattice with a spacing determined by Moruzzi *et al* (1978) of 5.27 au and at a temperature of 1200 K (local moment $\simeq 1.85\,\mu_B$) and FCC Ni on a lattice with spacing of 6.55 au and at a temperature 10 K (local moment $\simeq 0.22\,\mu_B$). Additionally, we have performed SCF KKR CPA calculations for FCC Fe on a lattice (measured by experiment) of 6.88 au at a temperature 1200 K. We found a local moment of $1.87\,\mu_B$ and the system had a Fermi energy (chemical potential) of 0.663 Ryd. The local densities of states for FCC Fe in this DLM model are shown in figure 4. We shall also describe details of the electronic structure from these calculations.

Figures 5, 6 and 7 show Bloch spectral functions for the three systems for a range of energies at various points along the Δ direction. On each plot the positions of the relevant 'pure up' and 'down' states are marked for easy analysis. At the Γ point shown in figure 5(*a*) the Bloch spectral function of BCC Fe has one broadened virtual-crystal Γ_{25}' state just below 0.7 Ryd and two smeared, 'locally exchange-split' Γ_{12} peaks at higher energies. Figure 6(*a*) shows the H point of BCC Fe and interpretation is somewhat different here—no 'split band' peaks are seen. There is one well defined, virtual-crystal H_{12} peak at about 0.45 Ryd and another broadened virtual-crystal H_{25} structure at higher energies. Thus the exchange splitting is $\boldsymbol{k}$ dependent, non-rigid and vanishes altogether at various points in the Brillouin zone. This is in marked contrast to the electronic structure at $T=0$. This collapse of the local exchange splitting can be tracked along the Δ direction as shown in figure 7(*a*). For example, halfway to the Brillouin zone boundary, with increasing energy, there are two virtual-crystal peaks, two split peaks and two further virtual-crystal peaks.

For the similar plots of FCC Fe, shown in figures 5(*b*), 6(*b*) and 7(*b*), qualitatively similar behaviour is seen although the various structures are more broadened owing to the larger disorder from the smaller band width. It is hoped that angle-resolved photoemission experiments using synchrotron radiation might test some of the features of these calculations, especially this loss of exchange splitting as a function of wavevector.

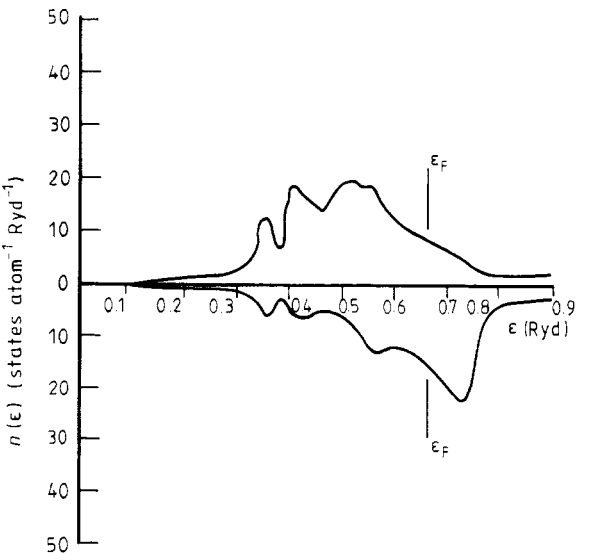

Figure 4. The densities of states for FCC Fe ($a=6.88$ au, $T=1200$ K).

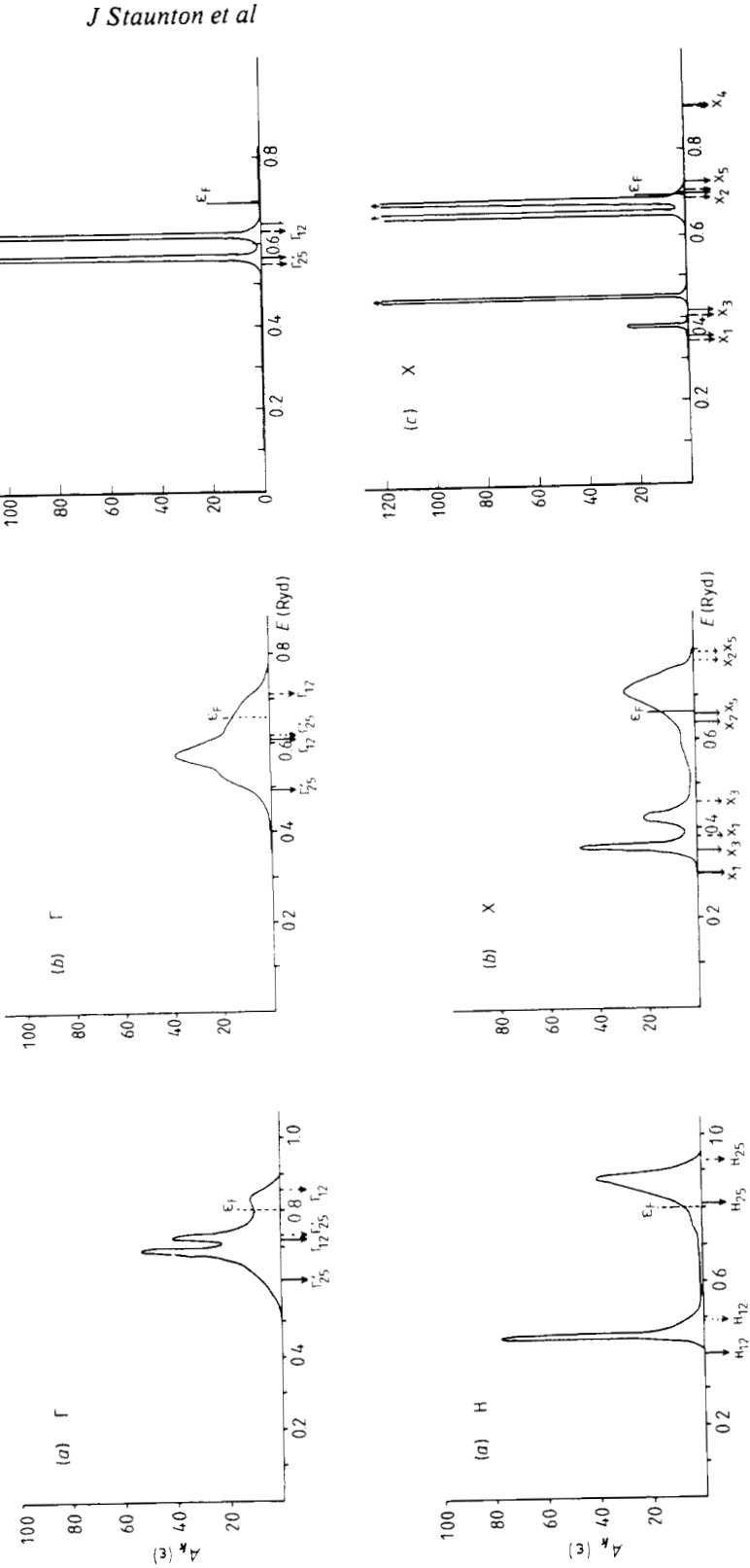

Figure 5. The Bloch spectral function $\bar{A}_B(\boldsymbol{k}, \varepsilon)$ (in states atom^{-1} Ryd^{-1}) as a function of energy at the Γ point (0, 0, 0) for (*a*) BCC Fe, (*b*) FCC Fe and (*c*) FCC Ni.

Figure 6. The Bloch spectral function $\bar{A}_B(\boldsymbol{k}, \varepsilon)$ as a function of energy for (*a*) BCC Fe at the H point (0, 0, 1), (*b*) FCC Fe at the X point (0, 0, 1) and (*c*) FCC Ni at the X point.

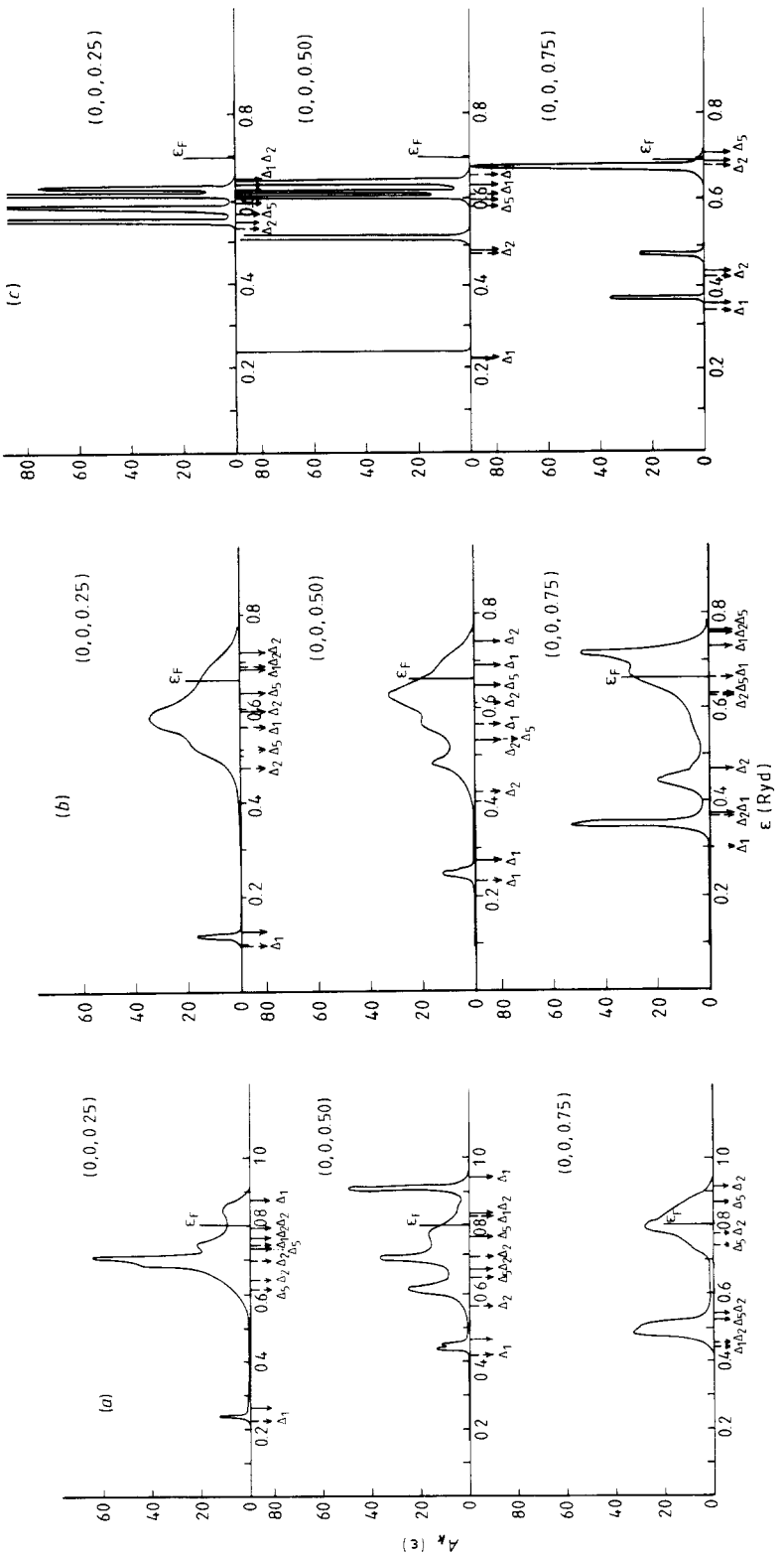

Figure 7. The Bloch spectral function at points (0, 0, 0.25), (0, 0, 0.5) and (0, 0, 0.75) in the Δ direction as a function of energy for (*a*) BCC Fe, (*b*) FCC Fe and (*c*) FCC Ni.

Our picture for nickel in this disordered local moment state as represented in figures 5(*c*), 6(*c*) and 7(*c*) is rather different. At all points along the Δ direction, a virtual-crystal description is adequate. At some points in $\boldsymbol{k}$ space and for some range of energies, the Bloch spectral function is very sharp, but in other regions the broadening is more pronounced.

It is now appropriate to return to the topic of the subtle establishment, or not, of a local moment by such self-consistent DLM calculations from the basis of the underlying electronic structure. If a 'split band' description is appropriate for the Bloch spectral function at all points in $\boldsymbol{k}$ and energy space, it is straightforward to see how a local moment is set up. As an example, we take the split peaks in the spectral function of BCC Fe at the Γ point (figure 5(*a*)): an electron with spin $+\frac{1}{2}$ will have a large amplitude on an 'up' site at energies near 0.73 Ryd. and then a large amplitude on a 'down' site at higher energies, above the Fermi energy, near 0.85 Ryd. Now an electron with spin $-\frac{1}{2}$ will see the 'inverse' picture—large amplitude on a 'down' site at energies near 0.73 Ryd and large amplitude on an 'up' site above the Fermi energy. Consequently, if this behaviour is apparent throughout the Brillouin zone, local moments will be established when the relevant $\boldsymbol{k}$- and energy-integrated quantity (equation (4.8)) is calculated. Electrons with spin $\frac{1}{2}$ and $-\frac{1}{2}$ with energy less than ε_F will be spatially separated: the former will be mainly on the up sites and the latter will reside preferentially on the down sites.

When the electronic structure is predominantly 'virtual-crystal'-like, as in nickel for example, the formation of a local moment is much more delicate. Here it is the asymmetry of the smearing of the peaks of the Bloch spectral function which is responsible for the small non-zero value of the local moment. So although the 'bands' of nickel in this model appear to be like Stoner–Wohlfarth ones, broadened by the magnetic disorder, they are capable of supporting a small local moment. This picture is roughly consistent with present angle-resolved (normal emission) photoemission data from measurements on nickel above its Curie temperature (Maetz *et al* 1982, Hopster *et al* 1983).

6. The 'Fermi surface' of Fe and Ni above the Curie temperature

Surfaces in $\boldsymbol{k}$ space can be constructed by calculating the Bloch spectral function at a particular energy along various directions in the Brillouin zone. In particular, in this section we describe such calculations at energies equal to the chemical potentials of the systems under study. These surfaces can be colloquially referred to as 'Fermi surfaces' and it is hoped that their features will eventually be studied by positron annihilation experiments (Berko 1979) upon iron and nickel above their Curie temperatures. Figures 8, 9 and 10 show slices of these Fermi surfaces in various symmetry directions for BCC Fe, FCC Fe and Ni respectively. In this paramagnetic state both electrons with spin $+\frac{1}{2}$ and those with spin $-\frac{1}{2}$ contribute to the same Fermi surface although its structure is strongly dependent on the magnetic disorder. In figure 8(*a*), $\bar{A}_B(\boldsymbol{k}, \varepsilon_F)$ in the Δ direction (Γ–H) is shown and its peaks are quite well defined on the scale of the Brillouin zone. (Once again, an analogous plot for an ordered system would be a set of delta functions.) The two outermost shoulders of the structure are of 'split' $\Delta_{2'}$ nature whilst the central peak is a virtual-crystal Δ_5-related peak. So, once more, there is a mixture of exchange-split and broadened, averaged features. Figure 8(*b*), showing $\bar{A}_B(\boldsymbol{k}, \varepsilon_F)$ in the Γ–N (Σ) direction, has one peak of broadened Σ_3 type and one rather sharp Σ_1 virtual-crystal spike. Along the Λ direction (Γ–P) there is simply one Λ_1-related virtual-crystal hump. Figures 9(*a*), (*b*) and (*c*) have a similar set of plots for FCC Fe with the noticeable difference that structure on the whole seems much less

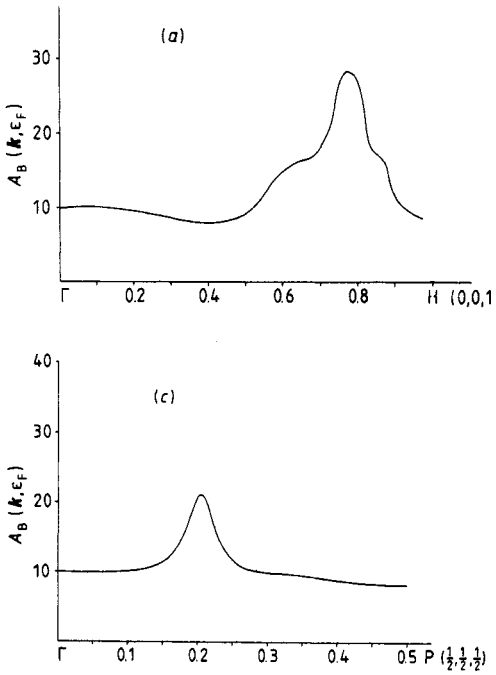

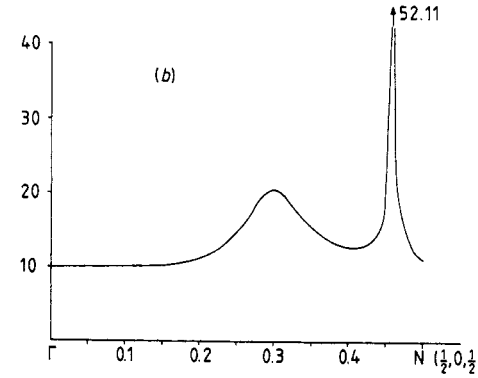

Figure 8. The Bloch spectral function at the Fermi energy as a function of distance to the Brillouin zone boundary for BCC Fe in the directions (*a*) Δ, (*b*) Σ and (*c*) Λ.

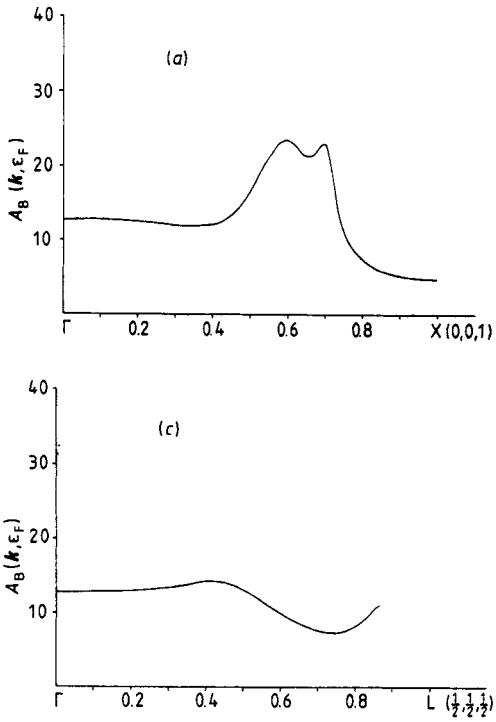

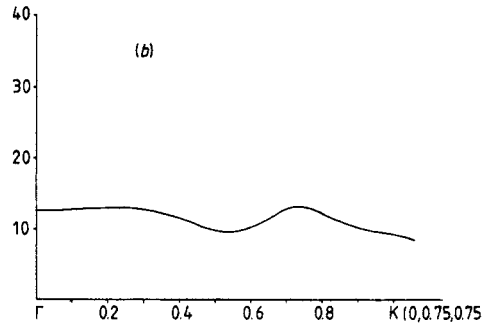

Figure 9. The Bloch spectral function at the Fermi energy for FCC Fe in the directions (*a*) Δ, (*b*) Σ and (*c*) Λ.

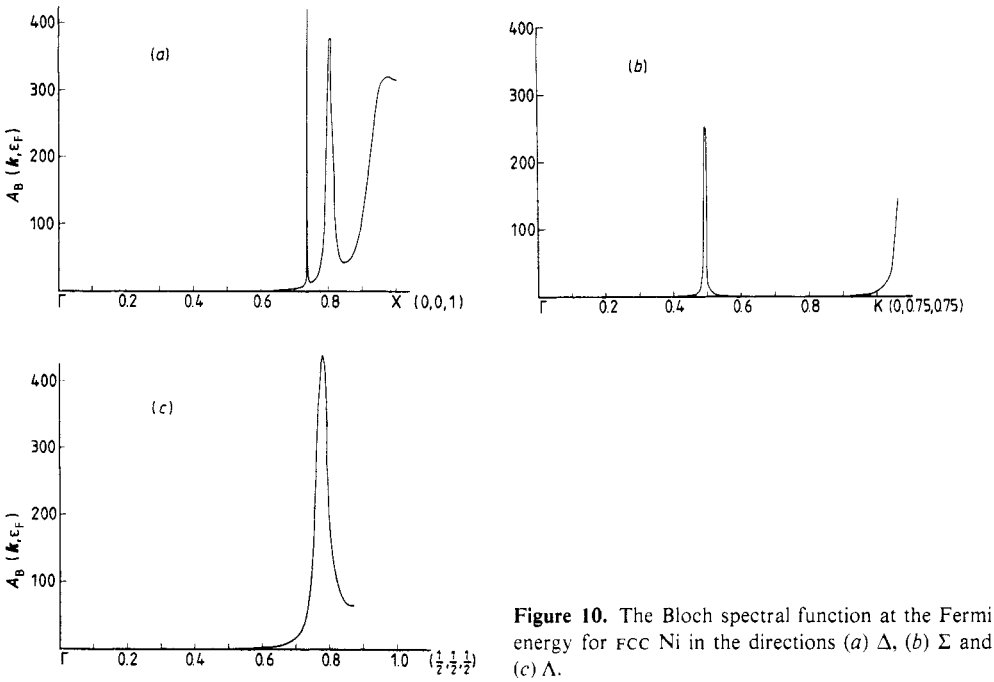

Figure 10. The Bloch spectral function at the Fermi energy for FCC Ni in the directions (*a*) Δ, (*b*) Σ and (*c*) Λ.

well defined. This is due to the fact that, on the scale of the band width, the magnetic disorder is larger. If the electronic structure calculations for BCC Fe were repeated on the lattice with the larger spacing determined by experiment ($a_0 = 5.43$ au) this greater disorder would also be apparent. In contrast, the 'Fermi surface' of nickel (figure 10) is well defined and is of a smeared, paramagnetic Stoner form. It is interesting, however, that the width of the broadening can vary with position in $\boldsymbol{k}$ space.

7. Conclusions

A discussion has been given on how local moments can form by different mechanisms derived from the electronic structures. At this point it is important to estimate what local magnetic order the electronic structure can 'drive' in itinerant magnets above their Curie temperatures. This is a first crucial step for a theory which calculates magnetic order and the 'driving' electronic structure self-consistently. In II a theory was derived for the paramagnetic wavevector-dependent spin susceptibility $\chi(q)$. Its full derivation includes both local moment 'flipping' effects as well as the variations in the magnitude of the local moments, reflecting the itinerant nature of the system. The transform of $\chi(q)$, i.e. χ_{ij}, gives the magnetisation–magnetisation correlation. Work is now in progress to carry out full studies of these quantities in Fe and Ni from the basis of our first-principles calculations. We shall now comment on the likely ranges of magnetic correlations which can be supported by the electronic structure we have described above.

Loosely speaking, the widths of the peaks in the Bloch spectral function at constant energy can be related to the coherence lengths ξ_k of the corresponding electronic 'states' in the averaged medium. In an averaged system an electronic 'state' has only finite coherence

corresponding to finite lifetimes. This can be intuitively understood in the following way: in such an averaged system (above the Curie temperature) a particle wave is scattered by 'up' and 'down' sites with equal probabilities. The resultant 'wave' is a random superposition of these two types of scattered waves and decays, on a scale related to the coherence length, as these two components interfere destructively. From the expression for $\chi(q)$ derived in II (equations (167) and (169)) the spatial range of χ_{ij} is governed by the product $\boldsymbol{\tau}^{c,ij}\boldsymbol{\tau}^{c,ji}$ where $\boldsymbol{\tau}^{c,ij}$ is a solution of equation (4.16). Now, the scattering path operator $\boldsymbol{\tau}^{c,ij}$ can be approximately written down as being proportional to $\exp(-|\boldsymbol{R}_i-\boldsymbol{R}_j|/\xi(\varepsilon))$ where $\xi(\varepsilon)$ is a $\boldsymbol{k}$-space-averaged coherence length at ε. Consequently it can be appreciated that the range of the magnetisation–magnetisation correlations is dominated by the widths of the peaks in the spectral functions.

Firstly it is noticeable that, for Fe, the peaks are quite well defined with widths ranging from $\frac{1}{5}$ to $\frac{1}{20}$ of the d-band width W for the constant-$\boldsymbol{k}$ Bloch spectral functions. Thus the corresponding, fairly propagating 'states' are long-lived compared with $\hbar/W$. Furthermore, by examining constant-energy Bloch spectral functions (figure 8) typically at the Fermi energy, the widths of those peaks range from $\frac{1}{2}$ to $\frac{1}{20}$ of the distance to the Brillouin zone boundary. From this, coherence lengths of 2 to 20 lattice spacings can be deduced. So, the suggestion is that in Fe the electronic structure derived from this mean-field description of the paramagnetic state may be capable of supporting a moderate degree of short-range magnetic order. In Ni, as seen from the Fermi surface plots in figure 10, the coherence lengths deduced range from many hundreds of lattice spacings for some sp-related states to a few tens of lattice spacings, and the magnetic structure is expected to show somewhat more short-range order than Fe with some reduction of this range by other aspects of the theory.

In conclusion, this paper has described the electronic structure basis of the mean-field theory of itinerant magnetism of II. It has defined a 'band structure at finite temperatures' and shown calculations for Fe and Ni in DLM states above their Curie temperatures. It is hoped that some of the predicted features may be tested by modern experiments which probe the electronic structure directly. In particular, it would be most interesting to see if Fe does, in fact, show a very wavevector-dependent, local exchange splitting above its Curie temperature. We have also emphasised the importance of studying the electronic structure directly both in the light of the current controversy over the nature of the paramagnetic state and with the aim of understanding the electronic mechanism underlying the spin fluctuations which, themselves, drive the ferromagnetic phase transition.

Appendix

Faulkner and Stocks (1980) have derived an expression for the Bloch spectral function $\bar{A}_B(\boldsymbol{k}, \varepsilon)$ for an averaged system with random disorder in terms of quantities which can be obtained from the corresponding KKR CPA calculation:

$$A_B(\boldsymbol{k}, \varepsilon) = -\frac{1}{\pi} \operatorname{Im} \sum_{LL'L''} [F^{cc}_{LL''}(\varepsilon)\tau^{c}_{L''L'}(\boldsymbol{k}, \varepsilon) - (F^{c}_{LL''}(\varepsilon) - F^{cc}_{LL''}(\varepsilon))\tau^{c,00}_{L''L'}(\varepsilon)]$$

where

$$F_{LL'} = D^{\alpha}_{L} R^{\alpha\alpha}_{LL'} \delta_{LL'}$$

$$F^{\alpha\beta}_{LL'} = D^{\alpha}_{L} R^{\alpha\beta}_{LL'} D^{\beta}_{L'}$$

and

$$D_L^{\alpha} = 1 + (t_{\alpha,L}^{-1} - t_{c,L}^{-1})\tau_{LL}^{c,00}$$

$$F_{LL'}^{c} = c_{\alpha}F_{LL'}^{\alpha} + c_{\beta}F_{LL'}^{\beta}$$

$$F_{LL'}^{cc} = c_{\alpha}^2 F_{LL'}^{\alpha\alpha} + c_{\alpha}c_{\beta}F_{LL'}^{\alpha\beta} + c_{\beta}c_{\alpha}F_{LL'}^{\beta\alpha} + c_{\beta}^2 F_{LL'}^{\beta\beta}$$

and $R_{LL'}^{\alpha\beta}$ are unit-cell integrals. For metals in the DLM state above their Curie temperatures $\alpha = \uparrow, \beta = \downarrow$ and $c_{\alpha} = c_{\beta} = \frac{1}{2}$.

References

von Barth U and Hedin L 1972 *J. Phys. C: Solid State Phys.* **5** 1629

Berko S 1979 *Proc. 5th Int. Conf. on Positron Annihilation, Lake Yamanaka, Japan* ed. R R Hasiguti and K Fujiwara (Sendai: Japan Inst. Met.)

Capellmann H 1974 *J. Phys. F: Met. Phys.* **4** 1966

—— 1979 *Z. Phys.* B **34** 29

Durham P J 1981 *J. Phys. F: Met. Phys.* **11** 2475

Edwards D M 1982 *J. Phys. F: Met. Phys.* **12** 1789

Faulkner J S and Stocks G M 1980 *Phys. Rev.* B **21** 3222

Fetter A L and Walecka J D 1971 *Quantum Theory of Many Particle Systems* (New York: McGraw-Hill)

Gordon B E A, Temmerman W M and Gyorffy B L 1981 *J. Phys. F: Met. Phys.* **11** 82

Gyorffy B L, Pindor A J, Staunton J, Stocks G M and Winter H 1985 *J. Phys. F: Met. Phys.* **15** 1337

Gyorffy B L and Stocks G M 1979 *Electrons in Disordered Metals and at Metallic Surfaces* ed. P Phariseau *et al* NATO ASI Series B **42** (New York: Plenum) p 89

Gunnarsson O 1976 *J. Phys. F: Met. Phys.* **6** 587

Hasegawa H 1979 *J. Phys. Soc. Japan* **46** 1504

Hopster H, Raue R, Guntherodt G, Kisker E, Clauberg R and Campagna M 1983 *Phys. Rev. Lett.* **51** 829

Hubbard J 1963 *Proc. R. Soc.* A **276** 238

—— 1979 *Phys. Rev.* B **20** 4584

—— 1981 *Phys. Rev.* B **23** 5974

Kadanoff L P and Baym G 1962 *Quantum Statistical Mechanics* (New York: Benjamin)

Korenman V, Murray J L and Prange R E 1977 *Phys. Rev.* B **16** 4032, 4048, 4058

Maetz C J, Gerhardt U, Dietz E, Ziegler A and Jellitto R J 1982 *Phys. Rev. Lett.* **48** 1686

Moriya T (ed.) 1981 *Electron Correlation and Magnetism in Narrow Band Systems* (Berlin: Springer)

Moruzzi V L, Janak J F and Williams A R 1978 *Calculated Electronic Properties of Metals* (New York: Pergamon)

Oguchi T, Terakura K and Hamada N 1983 *J. Phys. F: Met. Phys.* **13** 145

Pindor A J, Staunton J, Stocks G M and Winter H 1983 *J. Phys. F: Met. Phys.* **13** 979

Prange R E and Korenman V 1979 *Phys. Rev.* B **19** 4691

Rajagopal A K 1980 *Adv. Chem. Phys.* vol. 41 ed. I Prigogine and S A Rice (New York: Wiley) p 59

Szotek Z, Gyorffy B L, Stocks G M and Temmerman W M 1982 *Positron Annihilation* ed. P G Coleman *et al* (Amsterdam: North-Holland)

Temmerman W M, Gyorffy B L and Stocks G M 1978 *J. Phys. F: Met. Phys.* **8** 2461

Winter H and Stocks G M 1983 *Phys. Rev.* B **27** 882